ACS OMEGA

http://pubs.acs.org/journal/acsodf
Article

Quantum Emitters Induced by High Pressure and UV Laser Irradiation in Multilayer GaSe

Sinto Varghese, Sicheng Wang, Bimal Neupane, Bhojraj Bhandari, Yan Jiang, Roberto Gonzalez Rodriguez, Sergiy Krylyuk, Albert V. Davydov, Hao Yan, Yuanxi Wang, Anupama B. Kaul, Jingbiao Cui, and Yuankun Lin*

Cite This: *ACS Omega* 2025, 10, 7466−7473

Read Online

ACCESS | Metrics & More | Article Recommendations | Supporting Information

ABSTRACT: In this work, we report on defect generation in multilayer GaSe through hydrostatic pressure quenching and UV laser irradiation. The Raman line width from the UV 266 nm irradiated sample is much wider than that in pressure-quenched GaSe, corresponding to a wider defect energy distribution range in the former sample than the latter. After quenching from 11.2 GPa, three photoluminescence (PL) peaks from defect states are observed at 657, 681, and 695 nm at a low temperature of 93 K. Defect-related peaks at 649, 694, 750, and 774 nm also appear in low-temperature PL spectra after UV laser irradiation, with a nonmonotonous intensity dependence on irradiation duration. There are common features in defects produced by these two methods: the PL peaks with the lowest energy are sharp, and their PL intensities increase linearly with the excitation laser power and saturate above a certain excitation laser power. These two features are similar to those in defects for single-photon emission (SPE) in other 2D materials at even lower temperatures. Fluorescence lifetime imaging shows distinguished short (2.3 ns) and long (75.6 nm) lifetimes of the 695 nm PL line in pressure-quenched GaSe. The density functional theory predicts defect energy levels related to Se vacancy.

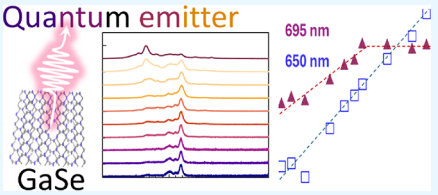

INTRODUCTION

The discovery of graphene initiated a new era in material science, opening the doors to the vast potential of two-dimensional (2D) materials.[1] These materials, characterized by their atomic thickness, exhibit unique physical and chemical properties that are absent in their bulk counterparts, making them highly desirable for applications in electronics, photonics, and quantum information technologies.[1] Among the family of 2D materials, transition metal dichalcogenides (TMDCs), monochalcogenides, and other layered compounds have gained significant interest due to their tunable band gaps, high carrier mobility, and strong light-matter interactions.[2−4] Gallium selenide (GaSe), a group-III monochalcogenide, stands out as a promising material with significant potential for applications in optoelectronics and quantum technologies due to its efficient second harmonic and THz generation,[5,6] high nonlinear coefficient and damage threshold,[7] up-conversion luminescence,[8] anisotropic Hall mobility,[9,10] and high on/off ratio.[10,11] GaSe, like many 2D materials, has a layered structure with weak van der Waals interactions between the layers,[12] allowing for easy exfoliation into atomically thin sheets. In the bulk form, it is a p-type semiconductor material[13] with a direct band gap of 2 eV[14] that transitions to an indirect band gap for a monolayer.[15] Furthermore, the tunability of electronic and optical properties of GaSe via external stimuli such as strain has made it a key material for defect engineering, a critical factor in the development of quantum emitters and single-photon sources.[16−18]

Defect engineering in 2D materials has emerged as a powerful tool for manipulating their intrinsic properties.[19−21] In GaSe, selenium (Se) vacancies are particularly interesting because they act as localized trapping centers for excitons,[22−24] which can give rise to enhanced photoluminescence (PL) and potential single-photon emission (SPE), a fundamental requirement for quantum information processing.[25] Unlike other 2D materials, e.g., MoS_2,[26] GaSe maintains a direct band gap in its multilayer form, making it highly effective for emission processes and an excellent candidate for achieving SPE. The defects in monolayers are often susceptible to oxidation under ambient conditions,[27] which limit their long-term stability for single-photon emitters. Multilayer GaSe offers an advantage in this regard: defects can be embedded beneath the surface of the sample, protecting them from environmental degradation and ensuring their stability.[19−21] This ability to maintain stable defects within multilayer structures makes GaSe particularly promising for SPE applications, providing a pathway to robust and durable quantum emitters.[28−30]

Received: January 22, 2025
Revised: February 5, 2025
Accepted: February 7, 2025
Published: February 14, 2025

Pressure is a thermodynamic variable that can significantly alter interatomic spacing in materials, which affects their electronic structure. In layered materials, pressure is particularly useful as it allows fine-tuning of intra- and interlayer interactions, making it a powerful tool to explore and manipulate their properties.[31−34] Recently, several studies have been conducted on the high-pressure behavior of 2D materials, highlighting advancements in the diamond anvil cell (DAC) technology for in situ measurements, particularly in atomically thin van der Waals materials.[35−37] Despite extensive studies on the pressure-dependent Raman modes of GaSe that revealed detailed vibrational dynamics and phase transitions, the PL properties of multilayers remain relatively underexplored, indicating a need for further research to fully understand the optical properties and electronic transitions of GaSe under high pressure.[34,38]

In addition to high-pressure techniques, ultraviolet (UV) laser irradiation has emerged as an effective method for generating vacancy defects in 2D layered materials.[21] In particular, recent studies have shown that UV irradiation in controlled environments can selectively create unpassivated vacancy defects that exhibit unique optical properties, including SPE, highlighting its potential for scalable quantum defect engineering in 2D materials.[27] Previous studies have already identified that laser irradiation can effectively induce defects in GaSe, such as point defects and localized exciton states, which significantly enhance its PL properties and contribute to advanced defect engineering strategies.[39] However, the exploration of UV laser irradiation effects on multilayer GaSe remains in its infancy, presenting a promising avenue for further investigation, particularly in optimizing defect configurations for SPE.

In this article, we report the generation of defects in multilayer GaSe using hydrostatic high pressure and UV laser irradiation. Several defect peaks have been observed in both samples produced through high-pressure quenching from 11.2 GPa and 266 nm UV irradiation. The PL peaks at the lowest energy level in both samples are narrow, and their intensity increases linearly and then saturates with further increasing excitation laser power, a characteristic of quantum emitters.

EXPERIMENTAL METHODS

Preparation of the Bulk GaSe sample. GaSe single crystals were produced using the vertical Bridgman technique, starting with a presynthesized polycrystalline GaSe charge. This charge was vacuum-sealed in a quartz ampule that had been graphitized. The melt was maintained at 990 °C for several hours to reach equilibrium before the ampule was moved through a temperature gradient at a slow rate of 0.4 mm/h. The ε-phase of GaSe was verified by X-ray diffraction.

Generation of Defects in Multilayer GaSe through 266 nm UV Laser Irradiation. A multilayer of GaSe was produced by exfoliating bulk GaSe using a Scotch tape followed by a thermal release tape in the final stage. Then it was transferred onto a SiO_2-coated Si substrate after pressing with a polydimethylsiloxane (PDMS) stamp. After this, the substrate, with GaSe attached, was heated to 100 °C to enable the thermal release of the tape to separate the sample onto the substrate. Then, 30 nm thickness of Al_2O_3 was coated by atomic layer deposition at 150 °C on the top of the sample to ensure the long-term stability of the sample. Next, the multilayer GaSe was subjected to UV irradiation by using a 266 nm laser (5 mW) for different exposure times. The refractive index of GaSe is relatively high. The Al_2O_3 coating can also improve the extraction efficiency if defect pairs act as an in-plane dipole.

Generation of Defects in Multilayer GaSe by Applying High Pressure. A multilayer GaSe sample was exfoliated from bulk GaSe using a Scotch tape, and the exfoliation process was repeated multiple times. Once the desired thickness was achieved, the sample was transferred to the thermal release tape. The thermal release tape was then heated to 100 °C to release free-standing multilayers flakes. Finally, the GaSe flakes were transferred to a diamond anvil cell (DAC) for high-pressure measurements. Hydrostatic pressure was applied to the samples using silicon oil as a pressure transition material by tightening the screws of the DAC.

Raman and PL Spectra. The Raman and PL measurements were conducted by using a Renishaw inVia Raman Microscope. These experiments were facilitated by a Cobolt Samba 532 nm laser coupled with a 50× objective lens (numerical aperture (NA) = 0.5) positioned at an 8.2 mm working distance. The 1800 lines/mm grating was utilized for the measurements to cover the full required wavelength range. Desired laser powers were achieved by combining neutral density filters with Cobolt Samba's laser power control software. In our optical setup, a 1 mW laser power equates to 0.59 $kWcm^{-2}$. For simplicity, all data were processed based on laser power rather than laser intensity. A heating/cooling stage (Linkam THMS600) was mounted on the microscope for in situ low-temperature Raman and PL analysis.

We also measured the Raman and PL spectra at room temperature using 473 and 785 nm lasers coupled with a 50× objective lens (NA = 0.5).

Fluorescence Lifetime Imaging (FLIM). The low-temperature FLIM and lifetime histograms for high-pressure-treated GaSe multilayer samples were investigated using a Micro Time 200 time-resolved confocal fluorescence microscope coupled with a heating/cooling stage (Linkam THMS600). A picosecond 405 nm laser was used for the excitation of PL. The laser intensity was set to 7, with a 0.6 neutral density filter used to lower the power, and an effective repetition rate of 2.5 MHz was chosen. The confocal microscope used a 20× objective lens (NA = 0.4) with a working distance of 12.0 mm. Data acquisition and analysis were carried out using the SymPho-Time 64 software.

Profilometer Measurements. The sample's height profile was assessed using a FILMETRICS Profilm 3D Profilometer with white light interferometry (WLI). To characterize the surface profiles, the envelope peak measurement parameter was selected under the single tab in the WLI settings.

DFT Calculations. The band structure was calculated using the density functional theory (DFT) as implemented in VASP using the Perdew−Burke−Ernzerhof (PBE) exchange-correlation functional and projector augmented wave (PAW) pseudopotentials. The cutoff for the kinetic energy of plane was 450 eV. A Γ-centered k-point grid was chosen such that its density is always equivalent to 10 × 10 × 1 for the Brillouin zone of a GaSe unit cell. The structure was optimized until an electronic convergence of 10^{-5} eV and a residual force of 0.02 eV/ Å were achieved.

RESULTS

High-Pressure-Induced Defects in Multilayer GaSe. Here, we report our study on a multilayer GaSe sample under

https://doi.org/10.1021/acsomega.5c00680
ACS Omega 2025, 10, 7466−7473

varying pressures. Figure S1 shows the surface topography image and height profile of the multilayer sample obtained by the profilometer. The thickness of the sample is 102 nm. The sample is then transferred into a DAC for in situ Raman measurements.

First, we analyzed the Raman spectra of our multilayer GaSe sample under different pressures. Figure 1a shows the

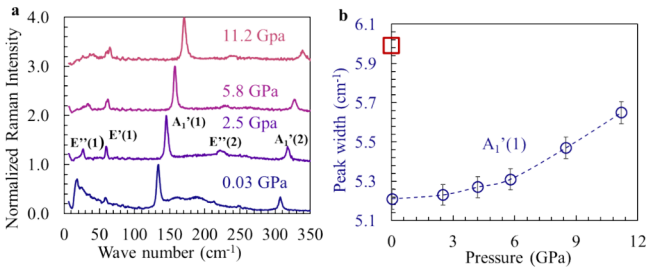

Figure 1. (a) Normalized Raman spectra of multilayer GaSe under varying pressures using 785 nm laser excitation (from 0.03 to 11.2 GPa). (b) Peak widths with increasing pressure for Raman $A_1'(1)$ mode. The red square is for the Raman line width after the release of pressure.

normalized Raman spectra of the sample at varying pressures ranging from 0.03 to 11.2 GPa. We observed Raman peaks at 20.59, 59.99, 134.13, 213.33, and 307.72 cm^{-1}. For a clearer representation, the spectrum at 2.5 GPa is included in the Supporting Information (Figure S2). The first five peaks are consistent with the previous reports and are identified as E"(1), E'(1), $A'_1(1)$, E"(2), and $A'_1(2)$, respectively.[34,40] The peaks at 495 and 705 cm^{-1} come from the silicone oil that has been used a pressure-transducing medium.[41] We also studied the shift in Raman peaks with respect to the pressure (Figure S3). The shift to higher wavenumbers is due to the compression of the crystal lattice under increasing pressure, which reduces the interatomic distances and strengthens the interatomic bonds. A noticeable change in the spectra shown in Figure 1a is the broadening of the peaks with increasing pressure. To further investigate this, we plotted the change in peak width for the $A_1'(1)$ mode as a function of pressure as shown in Figure 1b. The results indicate that the peak width increases with pressure. The broadening of the Raman peaks can be related to the distortion of hexagonal structures (movement of Ga or Se from the ideal lattice) as the hydrostatic pressure can drive the crystal toward an amorphous nature.[42−44] This behavior suggests an increasing disorder in the material under higher pressure; however, an irreversible transition to the amorphous state has not occurred yet because GaSe is stable under a hydrostatic pressure up to 20 GPa.[45] Figure S3d shows the Raman spectra of the sample after release from 11.2 GPa. It is notable that the line widths of the Raman lines do not return to their initial values after releasing the pressure. For example, the line widths for the $A'_1(1)$ and $A'_1(2)$ lines before and after pressure treatment are 5.21 and 5.99 cm^{-1}, and 4.43 and 6.45 cm^{-1}, respectively. This indicates that high pressure treatment induces permanent disorder of the crystal.

The pressure-induced defects can be revealed in PL spectral measurements. We analyzed the PL spectra of a multilayer GaSe sample before and after pressure treatment (Figure 2a). The red curve represents the PL spectrum prior to pressure application, showing a single prominent peak at 620 nm corresponding to the intrinsic band gap of the multilayer GaSe. Upon release from 9.8 GPa, the dark blue curve reveals an additional PL tail at higher wavelengths, although it is less intense than the band gap peak. After release from 11.2 GPa, as shown by the light blue curve, a broad defect PL peak centered at 650 nm becomes more pronounced, even surpassing the intensity of the direct band gap peak. The findings demonstrate that the application of high pressure can effectively generate defect states in the multilayer GaSe.

To understand more about the defect states, we conducted low-temperature PL measurements at 93 K. The PL spectrum of untreated GaSe at low temperature and low excitation (93 K, 0.1 mW), which shows only free exciton emission, is given in Figure S4. Figure 2b presents the PL spectra of pressure-treated GaSe measured at different excitation powers. Initially, we measured the spectrum at a laser power of 0.075 mW, where we observed an additional defect peak between 630 and 700 nm. We then reduced the laser power and measured the spectra at 0.05, 0.025, 0.0125, 0.01, 0.0075, 0.0050, 0.0025, 0.0017, and 0.0013 mW. Notably, the 650 nm peak becomes weaker relative to other PL peaks as the laser power decreases, with the 695 nm peak becoming dominant when the laser power is reduced below 0.05 mW (second curve from the top). For a more accurate analysis of peak behavior, we plotted the peak-fitted data in Figure 2c. Here, the blue curve represents the PL intensity of the 650 nm peak, while the purple curve represents the intensity of the 695 nm peak as a function of the laser power. From the plot, it is evident that the 650 nm peak intensity (I) exhibits a superlinear dependence on the laser

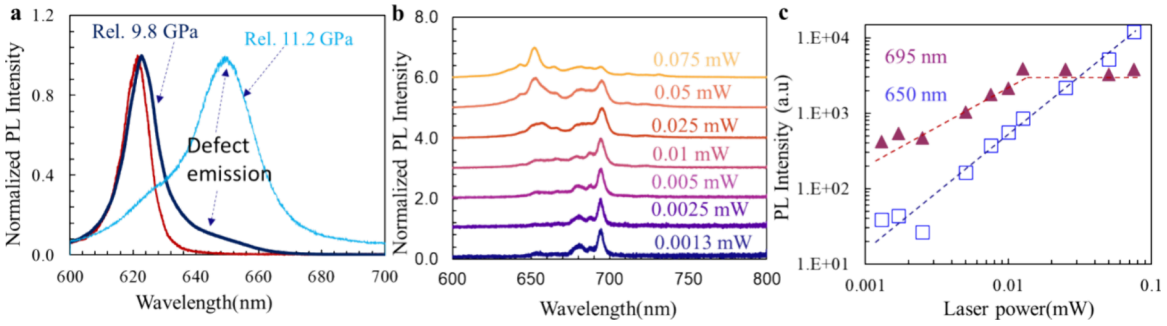

Figure 2. (a) Normalized PL spectra of multilayer GaSe at 300 K before and after pressure application with 473 nm laser excitation (red, 0 GPa; dark blue, 9.8 GPa; light blue, 11.2 GPa). (b) Low-temperature PL spectra at 93 K for the GaSe multilayer sample released from 11.2 GPa with different laser powers from 0.0013 to 0.075 mW. (c) PL intensities of the 650 nm peak (blue) and 695 nm peak (purple) with increasing laser power.

https://doi.org/10.1021/acsomega.5c00680
ACS Omega 2025, 10, 7466−7473

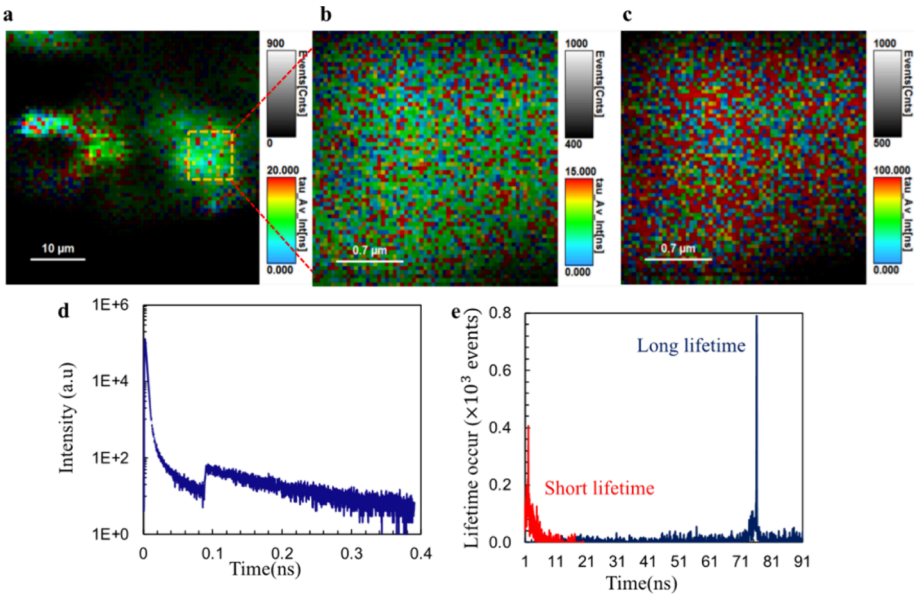

Figure 3. (a) FLIM in high-pressure applied multilayer GaSe sample excited by a 405 nm pulsed laser using a band-pass filter of 690 ± 10 nm. (b) Short-lifetime FLIM for the region of interest (ROI) (yellow square in panel a). (c) Long-lifetime FLIM for ROI. (d) PL decay and (e) its lifetime histogram for the ROI.

power (P) with $I \sim P^{1.51}$, while the 695 nm peak intensity increases sublinearly following $I \sim P^{0.93}$ and then saturates after 0.01 mW. Such PL saturation behavior is typically seen in localized energy states and is likely linked to highly confined systems.[27,46−48] In photon antibunching, one of the characteristics of SPE, the time between two successive photons is larger than a certain minimum value.[49] Thus, the brightness of SPE is limited by a certain number, explaining the intensity saturation behavior.[27] This behavior of the 695 nm peak, together with the narrow peak shape, suggests the possibility of SPE from this peak. Another group has already observed similar intensity-saturated defects in MoS_2 with SPE emission.[27] However, the SPE feature of defect PL at 695 nm in GaSe was not observed by second-order correlation $g^{(2)}(t = 0)$ measurement at 93 K. However, we cannot rule out the SPE due to the reasons below. Currently, the lowest-energy defect emission (695 nm) started to show up at a temperature of 103 K. We hypothesize that the temperature at 93 K in our measurement is not sufficiently low to observe the single photon emission. SPE was observed by other groups in multilayer GaSe at 10 K for the defect line near 1.881 ± 0.002 eV, which is at the lowest energy for defects.[25] The 695 nm line with unusual behavior is also at the lowest energy level in our study. There was no measurement[25] of the power dependence for the defect line near 1.881 ± 0.002 eV for a comparison with our results. One non-SPE emission line had $I \sim P^{1.3}$ representing the biexciton transition of the localized emission center, close to our $I \sim P^{1.51} \sim (P^{0.75})^2$ for 650 nm.[25] Our findings are further supported by the results of another group that previously observed single-photon emission (SPE) from multilayer GaSe.[28−30]

To investigate the carrier lifetime in high-pressure quenching-induced defect states in multilayer GaSe, we conducted lifetime measurements. Figure 3a presents the FLIM of a large area of the sample excited by a 405 nm pulsed laser. As seen from FLIM, the 695 nm peak appears in a certain region where defects are located. We selected a region of interest (ROI) (yellow square in Figure 3a) and generated FLIMs shown in Figure 3b,c using the intensity decay time between 0 and 0.08 ns, and 0.08 and 0.2 ns, respectively. Those decay time ranges were chosen based on the decay curve with the detector photo counting number above the noise level of 10 in Figure 3d. The spatial distributions of these two lifetime events are similar. The analysis of FLIM revealed two distinct lifetimes: a short lifetime of approximately 2.3 ns and a longer one of about 75.6 ns, as depicted in Figure 3e. We used perovskite $CsPbBr_3$ to test the system. The two separate segments in the PL decay curve were not observed for $CsPbBr_3$. Here is one of the possible explanations: the sharp peak at the beginning represents prompt PL; the long tail could arise from delayed PL from trap states that are common in materials with defects.[50] The pick-up of the 9.8 GPa sample from the hole of the gasket in DAC was not successful. Otherwise, more data from the 9.8 GPa sample can be compared for understanding the lifetime behavior.

UV Laser (266 nm) Irradiation-Induced Defects in Multilayer GaSe. In this study, we created defects in multilayer GaSe by using 266 nm UV laser irradiation. Figure S5 shows the surface topography image and height profile of the multilayer sample obtained by the profilometer. The thickness of the sample is determined by the height profile given by the profilometer (in Figure S5b) as 46 nm. First, we investigated how the duration of irradiation affects the PL emission. Figure 4a shows the PL spectra recorded after different irradiation times. The bottom curve represents the PL spectrum of the fresh sample without irradiation (0 min), which exhibits only a single peak at 620 nm, corresponding to the free exciton emission.[51] After 60 min of exposure, we observed the emergence of a broad peak at around 690 nm. Our analysis indicates that this peak likely originates from Se vacancies, as discussed in the theoretical section. The intensity of this new peak increased as the exposure time was extended. The defect peak intensity became stronger than that of free exciton after 4 h exposure in Figure 4a. The intensity ratio of the emerged peak over the free exciton peak reaches the maximum when the exposure time is 9 h, as shown in Figure

https://doi.org/10.1021/acsomega.5c00680
ACS Omega 2025, 10, 7466−7473

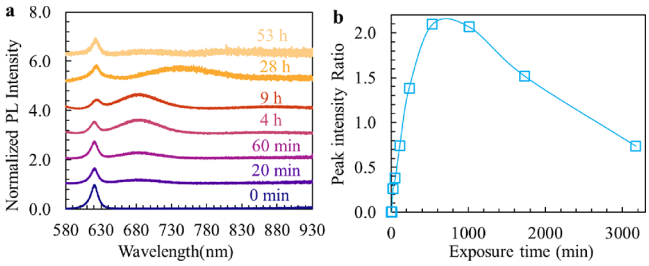

Figure 4. (a) Normalized PL spectra (at 300 K) of a multilayer GaSe sample after 266 nm UV laser irradiation for different exposure times. PL was excited using a 532 nm laser. (b) Intensity ratio of the 690 nm defect peak to the 620 nm band gap peak for different exposure times.

4b. However, with further increase in the exposure time, the peak intensity ratio gradually decreased. After 29 h of UV irradiation, PL signal-to-noise ratio significantly deteriorates as the defect concentration increases.

To better understand the positions of defects within the broad peak induced by 266 nm UV exposure, we investigated the low-temperature PL spectra of the sample at 93 K. For this analysis, we selected a different region in the same GaSe sample where we have a room-temperature defect PL peak stronger than the band gap peak. Figure S6 presents the surface topography and height profile of the selected multilayer piece, with the sample thickness determined by the profilometer (Figure S6b) to be 120 nm. Due to the thicker region of 120 nm than 46 nm in Figure 4, the intensity ratio of defect/620 nm should be close to that in the sample of 17 h (a little bit less than the maximum ratio in Figure 4b) considering the received energy dose of 266 nm laser per volume. Figure 5a shows the room-temperature PL spectrum at a laser power of 1 mW, where two peaks are evident: one at 620 nm, corresponding to the band gap, and another broad peak at 690 nm, attributed to defect states. Figure5b shows Raman spectra of the GaSe multilayer sample after 266 nm UV laser

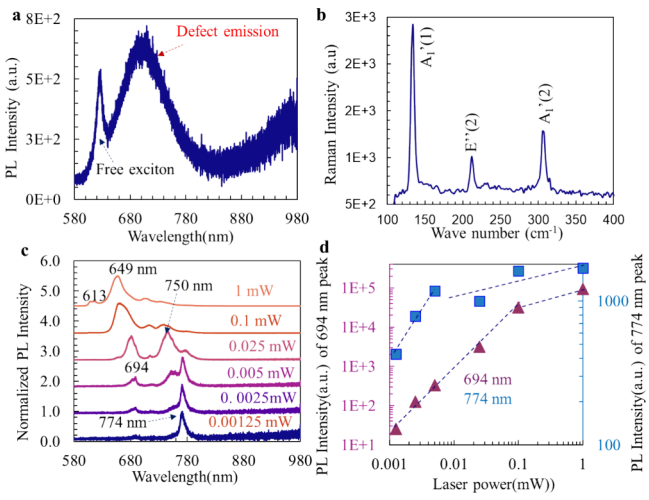

Figure 5. (a) PL spectrum of the 266 nm UV laser irradiated (53 h) multilayer GaSe sample from a damage-free spot (1 mW, 300 K). (b) Raman spectra of a GaSe multilayer sample after 266 nm UV laser irradiation for 53 h at 300 K. (c) Low-temperature PL spectra at 93 K for the GaSe multilayer sample with different laser powers from 0.00125 (bottom curve) to 1 mW (top curve). (d) PL Intensities of the 774 nm peak (blue, right *y* axis) and the 694 nm peak (purple, left *y* axis) with increasing laser powers.

irradiation for 53 h. Similarly to the pressure-treated GaSe samples, we observe a significant broadening of the Raman lines after UV irradiation.

The low-temperature PL measurements (Figure 5c) reveal additional defect-related peaks between 630 and 800 nm. At 1 mW, a peak at 649 nm dominates the spectrum. However, as the laser power was reduced, the 649 nm peak became barely visible and new peaks emerged, with the 694 and 774 nm peaks being particularly notable. The 694 nm peak matches the 695 nm defect peak observed in high-pressure-treated samples (Figure 2b). To further analyze the behavior of these peaks, we plotted their intensities versus excitation power in Figure 5d. The PL intensity of the 694 nm peak (plotted in purple) is shown on the right axis, and the 774 nm peak (plotted in blue) is shown on the left axis. The 694 nm peak exhibited a linear behavior as the laser power increased from 0.00125 to 0.1 mW, after which its intensity increased with a smaller slope. Measurements at even higher excitations were not possible due to the detector saturation.

Like the 694 nm peak, the 774 nm peak also exhibited a linear behavior initially, increasing steadily between 0.00125 and 0.005 mW. Beyond 0.005 mW, the PL intensity increases at a much smaller slope than before, as depicted by the blue curve in Figure 5d. The narrow peak shape and PL saturation of 774 nm triggered our interest of measuring $g^{(2)}(t = 0)$. However, the SPE feature at 774 nm in GaSe was not observed by $g^{(2)}(t = 0)$ measurement at 93 K. Comparing the defect PL at the lowest energy in Figures 2 and 5, both the high-pressure- and UV-irradiation-induced defects are promising for a further study for SPE.

DISCUSSION

The bulk GaSe material consists of Se−Ga−Ga−Se layers held together by van der Waals interactions. Previous studies suggest that at high pressures (around 16 GPa),[45] there is possibility of layer sliding and structural modifications, along with the possible occurrence of an ε-to-γ phase transition. The additional peaks observed in the PL spectra at 11.2 GPa, below the typical pressure for the ε-to-γ phase transition, suggest the involvement of defect formation in this process. We show in the following that it is the defect formation occurring at high pressure (around 11 GPa) that results in the irreversibility of the exciton PL and the appearance of additional PL peaks observed after releasing pressure.

A variety of defect species could be generated in multilayer GaSe under UV 266 nm irradiation. In addition, under hydrostatic pressure, GaSe hexagonal structures become distorted (displacement of Ga or Se from the ideal lattice), where an atom can dislodge to form an interstitial that either creates a Frenkel pair with a vacancy[52] or goes into the vdW gap. The formation energy of $V_{Se} < Se_i < (V_{Ga} + Ga_i) < (V_{Se} + Se_i)$ and Se_i is electronically inactive.[52] We considered V_{Se} and $(V_{Ga} + Ga_i)$ defects here as shown in Figure 6a,b, respectively, and calculated band structures of pristine GaSe, GaSe with Se vacancy, and GaSe with $V_{Ga} + Ga_i$ defects in Figure 6c−e. For both types of defects, we constructed a 5 × 5 × 1 supercell model of a V_{Se} in Figure 6a and a pair of $V_{Ga} + Ga_i$ defects in Figure 6b equivalent to a defect concentration of 0.5%. Since DFT band gaps are underestimated, here we will only focus on relative changes in band edge positions. Compared with the band structure of pristine GaSe in Figure 6c, a Se vacancy (Figure 6d) introduces three shallow defect bands labeled D_{v1}, D_{C1}, and D_{C2}, and $V_{Ga} + Ga_i$ defects (Figure 6e) result in three

https://doi.org/10.1021/acsomega.5c00680
ACS Omega 2025, 10, 7466−7473

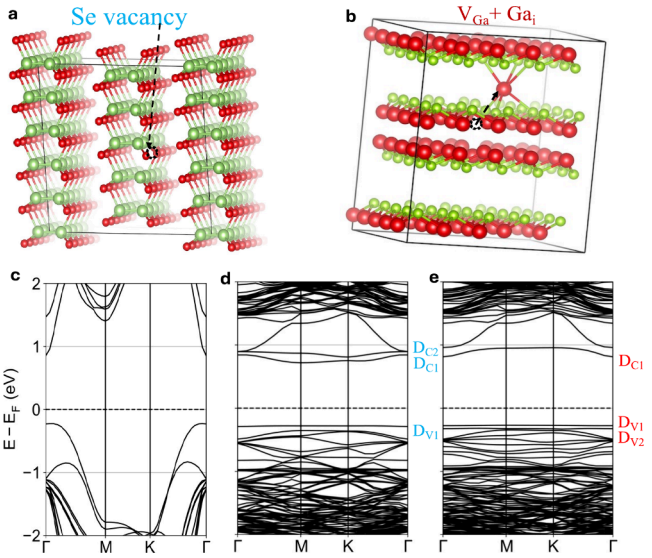

Figure 6. (a, b) Structure of a Se vacancy (a) and a first-neighbor Frenkel pair of V_{Ga} + Ga_i (Ga vacancy and Ga interstitial) (b) in bulk GaSe. (c–e) Band structure of pristine GaSe (c), GaSe with Se vacancy (d), and GaSe with V_{Ga} + Ga_i (e), where D_V represents the occupied defect level and D_C the unoccupied defect level.

defect bands at D_{C1}, D_{v1}, and D_{v2}. The free-exciton energy in the defect model of V_{Ga} + Ga_i blue-shifts in wavelength at the Γ point, and the defect energy levels barely change at the M and K points. In the defect model of Se vacancy, the energy of the free exciton is the same as one in pristine GaSe at the Γ point, and the defect energy level at M and K points shifts to a longer wavelength than the free exciton. Thus, the defect model of Se vacancy can explain the experimental data much better than the defect model of V_{Ga} + Ga_i. In Figure 6d, a gap decrease of ∼0.2 eV from pristine to defective GaSe is consistent with the ∼0.2 eV decrease between the measured free exciton PL peak at 623 nm and the defect PL peak at 695 nm.

CONCLUSIONS

In this study, we demonstrated controlled defect generation in multilayer GaSe through the application of hydrostatic pressure and UV irradiation. The low-temperature PL measurements have revealed the appearance of new PL peaks in both pressure-treated and UV-irradiated samples due to the generation of defects. For both samples, the new PL peaks at the lowest energies are dominant under low excitation power. Their intensities increase linearly and then saturate. Although SPE features have not been observed for these PL lines at 93 K, our results still suggest that high-pressure- and UV-irradiation-induced defects could serve as effective quantum emitters at even lower temperatures. DFT calculations revealed energy levels formed by Se vacancies that are responsible for the new PL lines. This work revealed convenient methods of quantum emitter generation instead of expensive ion-beam irradiation methods.

ASSOCIATED CONTENT

Supporting Information

The Supporting Information is available free of charge at https://pubs.acs.org/doi/10.1021/acsomega.5c00680.

Surface profile of the sample before applying pressure, Raman spectrum of the sample at 2.5 GPa pressure, change in Raman shift with increasing pressure and after removing pressure, normalized PL spectrum of the fresh sample at low temperature and low laser power (93K, 0.1 mW), surface profile of the sample before exposing 266 nm UV laser for 52 h, and surface profile of the damage-free sample surface after 266 nm UV laser exposure for 52 h (PDF)

AUTHOR INFORMATION

Corresponding Author

Yuankun Lin − *Department of Physics and Department of Electrical Engineering, University of North Texas, Denton, Texas 76203, United States;* orcid.org/0000-0001-5691-589X; Email: yuankun.lin@unt.edu

Authors

Sinto Varghese − *Department of Physics, University of North Texas, Denton, Texas 76203, United States;* orcid.org/0009-0006-3940-3845

Sicheng Wang − *Department of Chemistry, University of North Texas, Denton, Texas 76203, United States;* orcid.org/0000-0002-5224-5697

Bimal Neupane − *Department of Physics, University of North Texas, Denton, Texas 76203, United States*

Bhojraj Bhandari − *Department of Physics, University of North Texas, Denton, Texas 76203, United States*

Yan Jiang − *Department of Physics, University of North Texas, Denton, Texas 76203, United States*

Roberto Gonzalez Rodriguez − *Department of Physics, University of North Texas, Denton, Texas 76203, United States;* orcid.org/0000-0001-6849-1799

Sergiy Krylyuk − *Materials Science and Engineering Division, National Institute of Standards and Technology (NIST), Gaithersburg, Maryland 20899, United States;* orcid.org/0000-0003-4573-9151

Albert V. Davydov − *Materials Science and Engineering Division, National Institute of Standards and Technology (NIST), Gaithersburg, Maryland 20899, United States*

Hao Yan − *Department of Chemistry, University of North Texas, Denton, Texas 76203, United States;* orcid.org/0000-0003-4894-5620

Yuanxi Wang − *Department of Physics, University of North Texas, Denton, Texas 76203, United States*

Anupama B. Kaul − *Department of Electrical Engineering, University of North Texas, Denton, Texas 76203, United States; Department of Materials Science and Engineering, University of North Texas, Denton, Texas 76201, United States;* orcid.org/0000-0003-4052-8064

Jingbiao Cui − *Department of Physics, University of North Texas, Denton, Texas 76203, United States;* orcid.org/0000-0003-3408-1016

Complete contact information is available at: https://pubs.acs.org/10.1021/acsomega.5c00680

Notes

The authors declare no competing financial interest.

The authors declare no conflict of interest. This report was prepared as an account of work sponsored by an agency of the United States Government. Neither the United States Government nor any agency thereof, nor any of their

https://doi.org/10.1021/acsomega.5c00680
ACS Omega 2025, 10, 7466−7473

■ ACKNOWLEDGMENTS

S.K. and A.V.D. acknowledge the support from the Material Genome Initiative funding allocated to NIST. J.C. and Y.L. acknowledge the partial financial support from the U.S. National Science Foundation, grant number 2128367. A.K. and Y.L. acknowledge the partial financial support by the Department of Energy/National Nuclear Security Administration under Award DE-NA0004114. Y.W. acknowledges startup funds from UNT and partial support from NSF DMR-2340733.

■ REFERENCES

(1) Novoselov, K. S.; Geim, A. K.; Morozov, S. V.; Jiang, D.; Zhang, Y.; Dubonos, S. V.; Grigorieva, I. V.; Firsov, A. A. Electric Field Effect in Atomically Thin Carbon Films. *Science (1979)* **2004**, *306* (5696), 666−669.

(2) Iff, O.; Buchinger, Q.; Moczała-Dusanowska, M.; Kamp, M.; Betzold, S.; Davanco, M.; Srinivasan, K.; Tongay, S.; Antón-Solanas, C.; Höfling, S.; Schneider, C. Purcell-Enhanced Single Photon Source Based on a Deterministically Placed WSe_2 Monolayer Quantum Dot in a Circular Bragg Grating Cavity. *Nano Lett.* **2021**, *21* (11), 4715−4720.

(3) Klein, J.; Sigl, L.; Gyger, S.; Barthelmi, K.; Florian, M.; Rey, S.; Taniguchi, T.; Watanabe, K.; Jahnke, F.; Kastl, C.; Zwiller, V.; Jöns, K. D.; Müller, K.; Wurstbauer, U.; Finley, J. J.; Holleitner, A. W. Engineering the Luminescence and Generation of Individual Defect Emitters in Atomically Thin MoS_2. *ACS Photonics* **2021**, *8* (2), 669−677.

(4) Iff, O.; Tedeschi, D.; Martín-Sánchez, J.; Moczała-Dusanowska, M.; Tongay, S.; Yumigeta, K.; Taboada-Gutiérrez, J.; Savaresi, M.; Rastelli, A.; Alonso-González, P.; Höfling, S.; Trotta, R.; Schneider, C. Strain-Tunable Single Photon Sources in WSe_2 Monolayers. *Nano Lett.* **2019**, *19* (10), 6931−6936.

(5) Hirlimann, C.; Morhange, J.-F.; Chevy, A. Excitonic Resonant Second Harmonic in GaSe. *Solid State Commun.* **1989**, *69* (11), 1019−1022.

(6) Hohenleutner, M.; Langer, F.; Schubert, O.; Knorr, M.; Huttner, U.; Koch, S. W.; Kira, M.; Huber, R. Real-Time Observation of Interfering Crystal Electrons in High-Harmonic Generation. *Nature* **2015**, *523* (7562), 572−575.

(7) Vodopyanov, K. L.; Mirov, S. B.; Voevodin, V. G.; Schunemann, P. G. Two-Photon Absorption in GaSe and $CdGeAs_2$. *Opt. Commun.* **1998**, *155* (1−3), 47−50.

(8) Fan, Y.; Bauer, M.; Kador, L.; Allakhverdiev, K. R.; Salaev, E. Yu. Photoluminescence Frequency Up-Conversion in GaSe Single Crystals as Studied by Confocal Microscopy. *J. Appl. Phys.* **2002**, *91* (3), 1081−1086.

(9) Augelli, V.; Manfredotti, C.; Murri, R.; Vasanelli, L. Hall-Mobility Anisotropy in GaSe. *Phys. Rev. B* **1978**, *17* (8), 3221−3226.

(10) Late, D. J.; Liu, B.; Luo, J.; Yan, A.; Matte, H. S. S. R.; Grayson, M.; Rao, C. N. R.; Dravid, V. P. GaS and GaSe Ultrathin Layer Transistors. *Adv. Mater.* **2012**, *24* (26), 3549−3554.

(11) Kim, W.; Li, C.; Chaves, F. A.; Jiménez, D.; Rodriguez, R. D.; Susoma, J.; Fenner, M. A.; Lipsanen, H.; Riikonen, J. Tunable Graphene−GaSe Dual Heterojunction Device. *Adv. Mater.* **2016**, *28* (9), 1845−1852.

(12) Capozzi, V. Direct and Indirect Excitonic Emission in GaSe. *Phys. Rev. B* **1981**, *23* (2), 836−840.

(13) Capozzi, V.; Montagna, M. Optical Spectroscopy of Extrinsic Recombinations in Gallium Selenide. *Phys. Rev. B* **1989**, *40* (5), 3182−3190.

(14) Ghalouci, L.; Benbahi, B.; Hiadsi, S.; Abidri, B.; Vergoten, G.; Ghalouci, F. First Principle Investigation into Hexagonal and Cubic Structures of Gallium Selenide. *Comput. Mater. Sci.* **2013**, *67* (1), 73−82.

(15) Ben Aziza, Z.; Pierucci, D.; Henck, H.; Silly, M. G.; David, C.; Yoon, M.; Sirotti, F.; Xiao, K.; Eddrief, M.; Girard, J. C.; Ouerghi, A. Tunable Quasiparticle Band Gap in Few-Layer GaSe/Graphene van Der Waals Heterostructures. *Phys. Rev. B* **2017**, *96* (3), 1−8.

(16) Wu, Y.; Fuh, H. R.; Zhang, D.; Coileáin, C.; Xu, H.; Cho, J.; Choi, M.; Chun, B. S.; Jiang, X.; Abid, M.; Abid, M.; Liu, H.; Wang, J. J.; Shvets, I. V.; Chang, C. R.; Wu, H. C. Simultaneous Large Continuous Band Gap Tunability and Photoluminescence Enhancement in GaSe Nanosheets via Elastic Strain Engineering. *Nano Energy* **2017**, *32* (1), 157−164.

(17) Zhang, D.; Jia, T.; Dong, R.; Chen, D. Temperature-Dependent Photoluminescence Emission from Unstrained and Strained GaSe Nanosheets. *Materials* **2017**, *10* (11), 1282.

(18) Maeso, D.; Pakdel, S.; Santos, H.; Agraït, N.; Palacios, J. J.; Prada, E.; Rubio-Bollinger, G. Strong Modulation of Optical Properties in Rippled 2D GaSe via Strain Engineering. *Nanotechnology* **2019**, *30* (24), No. 24LT01.

(19) Lin, Y.; Hathaway, E.; Habis, F.; Wang, Y.; Rodriguez, R. G.; Alnasser, K.; Hurley, N.; Cui, J. Enhanced Emission from Defect Levels in Multilayer MoS_2. *Adv. Opt Mater.* **2022**, *10* (19), 1−9.

(20) Lin, Y.; Hurley, N.; Kamau, S.; Hathaway, E.; Jiang, Y.; Rodriguez, R. G.; Varghese, S.; Krylyuk, S.; Davydov, A. V.; Wang, Y.; Kaul, A.; Cui, J. Strain-Activated Stimulated Emission from Multilayer $MoSe_2$ in a Narrow Operation Window. *Phys. Status Solidi RRL* **2024**, *18* (2), 1−8.

(21) Varghese, S.; Hurley, N.; Kamau, S.; Jiang, Y.; Rodriguez, R. G.; Bhandari, B.; Lyu, T.; Yan, H.; Wang, Y.; Kaul, A. B.; Cui, J.; Lin, Y. Thermal-Strain-Enabled Enhanced Emission from UV Laser-Induced Defect Levels near the Surface of Multilayer MoS_2. *ACS Applied Optical Materials* **2024**, *2* (8), 1721−1729.

(22) Taylor, R. A.; Rayn, J. F. Time-Resolved Exciton Photoluminescence in GaSe and GaTe. *Journal of Physics C: Solid State Physics* **1987**, *20* (36), 6175−6187.

(23) Hopkinson, D. G.; Zólyomi, V.; Rooney, A. P.; Clark, N.; Terry, D. J.; Hamer, M.; Lewis, D. J.; Allen, C. S.; Kirkland, A. I.; Andreev, Y.; Kudrynskyi, Z.; Kovalyuk, Z.; Patanè, A.; Fal'ko, V. I.; Gorbachev, R.; Haigh, S. J. Formation and Healing of Defects in Atomically Thin GaSe and InSe. *ACS Nano* **2019**, *13* (5), 5112−5123.

(24) Cohen, A.; Lewis, D. K.; Huang, T.; Sharifzadeh, S. Localized Excitons in Defective Monolayer Germanium Selenide. *Phys. Rev. Mater.* **2020**, *4* (7), 1−7.

(25) Tonndorf, P.; Schwarz, S.; Kern, J.; Niehues, I.; Del Pozo-Zamudio, O.; Dmitriev, A. I.; Bakhtinov, A. P.; Borisenko, D. N.; Kolesnikov, N. N.; Tartakovskii, A. I.; Michaelis de Vasconcellos, S.; Bratschitsch, R. Michaelis de Vasconcellos, S.; Bratschitsch, R. Single-Photon Emitters in GaSe. *2d Mater.* **2017**, *4* (2), No. 021010.

(26) Ahmad, S.; Mukherjee, S. A Comparative Study of Electronic Properties of Bulk MoS2 and Its Monolayer Using DFT Technique: Application of Mechanical Strain on MoS2Monolayer. *Graphene* **2014**, *03* (04), 52−59.

(27) Wang, W.; Jones, L. O.; Chen, J. S.; Schatz, G. C.; Ma, X. Utilizing Ultraviolet Photons to Generate Single-Photon Emitters in Semiconductor Monolayers. *ACS Nano* **2022**, *16* (12), 21240−21247.

(28) Luo, W.; Lawrie, B. J.; Puretzky, A. A.; Tan, Q.; Gao, H.; Lingerfelt, D. B.; Eichman, G.; Mcgee, E.; Swan, A. K.; Liang, L.; Ling,

https://doi.org/10.1021/acsomega.5c00680
ACS Omega 2025, 10, 7466−7473

X. Imaging Strain-Localized Single-Photon Emitters in Layered GaSe below the Diffraction Limit. *ACS Nano* **2023**, *17* (23), 23455−23465.
(29) Luo, W.; Puretzky, A.; Lawrie, B.; Tan, Q.; Gao, H.; Swan, A. K.; Liang, L.; Ling, X. Improving Strain-Localized GaSe Single Photon Emitters with Electrical Doping. *Nano Lett.* **2023**, *23* (21), 9740−9747.
(30) Luo, W.; Puretzky, A. A.; Lawrie, B. J.; Tan, Q.; Gao, H.; Chen, Z.; Sergienko, A. V.; Swan, A. K.; Liang, L.; Ling, X. Deterministic Localization of Strain-Induced Single-Photon Emitters in Multilayer GaSe. *ACS Photonics* **2023**, *10* (8), 2530−2539.
(31) Clarke, R.; Uher, C. High Pressure Properties of Graphite and Its Intercalation Compounds. *Adv. Phys.* **1984**, *33* (5), 469−566.
(32) Besson, J. M. High-Pressure Effects in Layer Semiconductors. *Il Nuovo Cimento B Series 11* **1977**, *38* (2), 478−485.
(33) Gauthier, M.; Polian, A.; Besson, J. M.; Chevy, A. Optical Properties of Gallium Selenide under High Pressure. *Phys. Rev. B* **1989**, *40* (6), 3837−3854.
(34) Pellicer-Porres, J. Understanding Layered Compounds under High Pressure. *J. Appl. Phys.* **2024**, *135* (9), 1−18.
(35) Pimenta Martins, L. G.; Comin, R.; Matos, M. J. S.; Mazzoni, M. S. C.; Neves, B. R. A.; Yankowitz, M. High-Pressure Studies of Atomically Thin van Der Waals Materials. *Appl. Phys. Rev.* **2023**, *10* (1), 1−42.
(36) Pei, S.; Wang, Z.; Xia, J. High Pressure Studies of 2D Materials and Heterostructures: A Review. *Mater. Des* **2022**, *213*, No. 110363.
(37) Zhang, L.; Tang, Y.; Khan, A. R.; Hasan, M. M.; Wang, P.; Yan, H.; Yildirim, T.; Torres, J. F.; Neupane, G. P.; Zhang, Y.; Li, Q.; Lu, Y. 2D Materials and Heterostructures at Extreme Pressure. *Advanced Science* **2020**, *7* (24), 1−26.
(38) Zheng, Y. L.; Li, L.; Li, F. F.; Zhou, Q.; Cui, T. Pressure-Dependent Phonon Scattering of Layered GaSe Prepared by Mechanical Exfoliation. *Chin. Phys. Lett.* **2020**, *37* (8), No. 088201.
(39) Mozol, P. E.; Skubenko, N. A.; Skubenko, P. A.; Gnatenko, Yu. P.; Salkov, E. A.; Kovalyuk, Z. D. Effect of Laser Irradiation on Low-Temperature Photoconductivity and Photoluminescence Spectra of Gallium Selenide. *physica status solidi (b)* **1989**, *153* (2), 667−673.
(40) Osiekowicz, M.; Staszczuk, D.; Olkowska-Pucko, K.; Kipczak; Grzeszczyk, M.; Zinkiewicz, M.; Nogajewski, K.; Kudrynskyi, Z. R.; Kovalyuk, Z. D.; Patané, A.; Babiński, A.; Molas, M. R. Resonance and Antiresonance in Raman Scattering in GaSe and InSe Crystals. *Sci. Rep* **2021**, *11* (1), 1−8.
(41) Chen, X.; Lou, H.; Zeng, Z.; Cheng, B.; Zhang, X.; Liu, Y.; Xu, D.; Yang, K.; Zeng, Q. Structural Transitions of 4:1 Methanol-Ethanol Mixture and Silicone Oil under High Pressure. *Matter and Radiation at Extremes* **2021**, *6* (3), 1−6.
(42) Lin, Y.; Li, Y.; Xu, Y.; Lan, G.; Wang, H. Raman-Scattering Study on Pressure Amorphization of LiNbO3 Crystal. *J. Appl. Phys.* **1995**, *77* (7), 3584−3585.
(43) Lin, Y.; Lan, G.; Wang, H. An Irreversible Pressure-Induced Amorphization in LiTaO3 Crystal. *Solid State Commun.* **1994**, *91* (11), 879−881.
(44) Lin, Y.; Lan, G.; Wang, H. Pressure-Induced Amorphization of Crystalline Pb5Ge3O11. *Solid State Commun.* **1993**, *86* (2), 99−101.
(45) Diep, N. Q.; Wu, S. K.; Liu, C. W.; Huynh, S. H.; Chou, W. C.; Lin, C. M.; Zhang, D. Z.; Ho, C. H. Pressure Induced Structural Phase Crossover of a GaSe Epilayer Grown under Screw Dislocation Driven Mode and Its Phase Recovery. *Sci. Rep* **2021**, *11* (1), 1−10.
(46) Klein, J.; Lorke, M.; Florian, M.; Sigger, F.; Sigl, L.; Rey, S.; Wierzbowski, J.; Cerne, J.; Müller, K.; Mitterreiter, E.; Zimmermann, P.; Taniguchi, T.; Watanabe, K.; Wurstbauer, U.; Kaniber, M.; Knap, M.; Schmidt, R.; Finley, J. J.; Holleitner, A. W. Site-Selectively Generated Photon Emitters in Monolayer MoS_2 via Local Helium Ion Irradiation. *Nat. Commun.* **2019**, *10* (1), 1−8.
(47) Castelletto, S.; Boretti, A. Silicon Carbide Color Centers for Quantum Applications. *Journal of Physics: Photonics* **2020**, *2* (2), No. 022001.
(48) Ma, X.; Adamska, L.; Yamaguchi, H.; Yalcin, S. E.; Tretiak, S.; Doorn, S. K.; Htoon, H. Electronic Structure and Chemical Nature of Oxygen Dopant States in Carbon Nanotubes. *ACS Nano* **2014**, *8* (10), 10782−10789.
(49) Aharonovich, I.; Englund, D.; Toth, M. Solid-State Single-Photon Emitters. *Nat. Photonics* **2016**, *10* (10), 631−641.
(50) Eremchev, I. Yu.; Tarasevich, A. O.; Kniazeva, M. A.; Li, J.; Naumov, A. V.; Scheblykin, I. G. Detection of Single Charge Trapping Defects in Semiconductor Particles by Evaluating Photon Antibunching in Delayed Photoluminescence. *Nano Lett.* **2023**, *23* (6), 2087−2093.
(51) Wei, C.; Chen, X.; Li, D.; Su, H.; He, H.; Dai, J.-F. Bound Exciton and Free Exciton States in GaSe Thin Slab. *Sci. Rep* **2016**, *6* (1), 1−6.
(52) Deák, P.; Han, M.; Lorke, M.; Tabriz, M. F.; Frauenheim, T. Intrinsic Defects of GaSe. *J. Phys.: Condens. Matter* **2020**, *32* (28), 285503−5.

https://doi.org/10.1021/acsomega.5c00680
ACS Omega 2025, 10, 7466−7473